ADVANCED HEALTHCARE MATERIALS
www.advhealthmat.de

A Novel Anti-Coagulative Nanocomplex in Delivering miRNA-1 Inhibitor Against Microvascular Obstruction of Myocardial Infarction

Ting Hong, Yazhong Wei, Xiaomei Xue, Yongyong Li, Haiqing Dong, Xiaoyu Guo, Xueyin Shi, and Bin He**

Great progress has been made in miRNA nanodelivery for the treatment of myocardial infarction (MI). However, miRNA nanodelivery within the infarct is impeded by microvascular obstruction as a local circulatory disorder caused by microthrombus formation in microvessels. Knowing that low molecular weight heparin (LMWH) can effectively prevent microthrombus formation in microcirculation, it is hypothesized whether surface modification of the nanocarrier with LMWH can overcome microvascular obstruction in the infarct area for better miRNA delivery. Herein, a novel nanocomlex consisting of dendrigraft poly-L-lysine (DGL)-loaded miR-1 inhibitor as the core to decrease apoptosis of cardiomyocytes and LMWH as the shell to overcome microvascular obstruction of the infarct area is developed. The results show that this anti-coagulative nanocomlex is able to reduce microthrombus formation in microvessels and inhibit blood-coagulation factor Xa, thereby overcoming microvascular obstruction in the infarct area. In addition, it further enhances the uptake of miR-1 inhibitor within the infarct and decreases myocardiocyte apoptosis, thus improving the cardiac function and attenuating the myocardial fibrosis. In conclusion, modification of DGL-loaded miR-1 inhibitor with LMWH helps overcome microvascular obstruction in delivering the drug to the infarct area, thus providing a promising therapeutic strategy for achieving a better therapeutic outcome of MI.

1. Introduction

Acute myocardial infarction (MI) is the leading cause of morbidity, mortality, and disability worldwide.[1] MicroRNA (miRNA)-based therapy is an avenue being explored for the treatment of MI. A number of miRNA nanodelivery systems have been engineered, including targeted modified and synthetic nanoparticles (NPs), which overcome the drawbacks of local injection of miRNAs.[2] For instance, a work presents a therapeutic strategy to manipulate macrophage phenotype using NP delivery of miRNA-21 for cardiac repair.[3] To inhibit the role of miR-1 in promoting myocardial apoptosis in ischemic tissues,[4] we have previously encapsulated anti-miR-1 antisense oligonucleotide (AMO-1) into the cationic polymer-dendrigraft poly-L-lysine (DGL) based nanovector, which conjugated with an myocardium-targeted peptide, for the treatment of MI.[5] Despite the improved therapeutic outcome, the delivery efficiency of miRNA was compromised by microvascular obstruction of MI.

Microvascular obstruction is a phenomenon of vascular microthrombosis caused by constant formation of emboli in microvessels around the infarct area, which often results in severe cardiomyocyte death and negative progressive ventricular remodeling.[6] The formation process is as follows. MI initiates a sudden complete or partial obstruction of an coronary artery caused by thrombi superimposed on disrupted atherosclerotic plaque,[7] which represents a "solid-state" stimulus to both thrombosis and coagulation; these pathways mentioned above reinforce each other, further heightening blood thrombogenicity.[8] Continuous superimpositon of thrombi at the site of atherosclerosis and a large number of thrombi formed in downstream functional capillaries narrow the remaining vascular lumen, thus seriously affecting blood supply of the myocardial tissue.[9] These may also be the reason why the targeted modified NPs are still difficult to be delivered to the target site in vivo, although they exhibited high targeting and transfection efficiency in vitro.[10] This difficulty can be partially reflected by the weak accumulation of micro-RNA within the infarct of MI.[5] It thus necessitates the development of a novel approach to address the above issue.

Anticoagulation is a clinical approach that can effectively prevent thrombus formation.[11] Low molecular weight heparin

T. Hong, Y. Wei, Dr. X. Xue, X. Guo, Prof. X. Shi, Prof. B. He
Department of Anesthesiology and SICU
Xinhua Hospital
School of Medicine Shanghai Jiao Tong University
Shanghai 200092, China
E-mail: xiaomeixue_xinhua@163.com; hebin@xinhuamed.com.cn
Prof. Y. Li, Prof. H. Dong
Institute for Biomedical Engineering & Nano Science
Shanghai East Hospital
Tongji University School of Medicine
Shanghai 200092, China

The ORCID identification number(s) for the author(s) of this article can be found under https://doi.org/10.1002/adhm.201901783

DOI: 10.1002/adhm.201901783

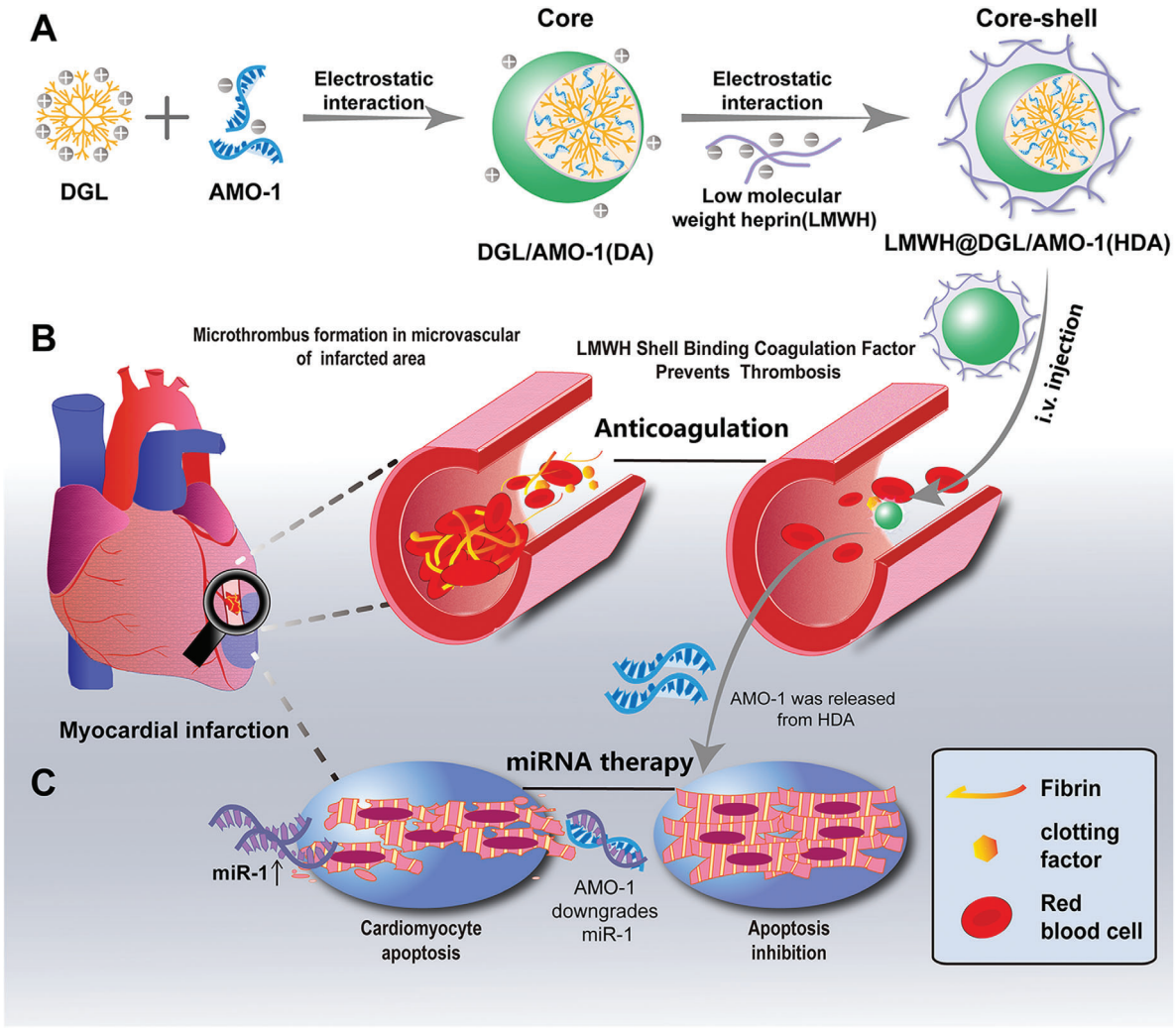

Figure 1. Schematic illustration of the preparation of the LMWH@DGL/AMO-1 (HDA) and the therapeutic mechanisms of HDA to treat MI. A) Core and core–shell NPs design. B) HDA NPs are taken to the coronary artery to prevent thrombosis. C) HDA NPs are further taken up by ischemic cardiac cells to downregulate miR-1 expression. LMWH@DGL/AMO-1: HDA; LMWH@DGL: HD; DGL/AMO-1: DA; MI: myocardial infarction.

(LMWH) is a commonly used anticoagulant for MI, knowing that it can produce an anticoagulative effect by enhancing the antithrombin activity.[10] Compared with unfractionated (higher molecular weight) heparin, LMWH exhibits a reduced binding capacity to protein and cells and also a longer plasma half-life.[13] It has been documented that LMWH coating could resist phagocytosis by inhibiting the activation of complement at different stages and creating a steric barrier in blood.[14] Additionally, it is also a negatively charged polysaccharide macromolecule that can strongly interact with polycations.[15] These merits make LMWH a suitable modifier for miRNA nanocarriers, for the purpose of improving microvascular obstruction, a critical need to improve mRNA accumulation in the infarct area.

In the present study, we developed a novel type of low-cytotoxic core–shell nanocarrier with a DGL core and a LMWH shell for delivering AMO-1. Such unique NPs with a LMWH shell proved to have greatly improved stability in serum and excellent dispersibility. First, the LMWH shell is expected to exert a basic anticoagulative effect to prevent further microthrombosis, and then AMO-1 compressed in DGL will neutralize miR-1 and thereby attenuate cardiomyocyte apoptosis. The ability of the nanocomplex to promote neovascularization and improve ventricular remodeling after MI has also been investigated. The novel NPs could improve microvascular obstruction encountered in the treatment of MI with miRNA.

2. Results and Discussion

2.1. Synthesis and Characterization of HDA

Two-step electrostatic interaction was used to synthesize HDA NPs. In the first step, as shown in **Figure 1**A, AMO-1 was compressed into a positively charged DGL. When the weight ratio of DGL to AMO-1 was 1:1, AMO-1 was fully condensed by DGL, and the optimal feed ratio of AMO-1 to DGL was 1:1.5 for the next reaction. As shown in Figure S1, Supporting Information, the DA particles size increased sharply after 48h.

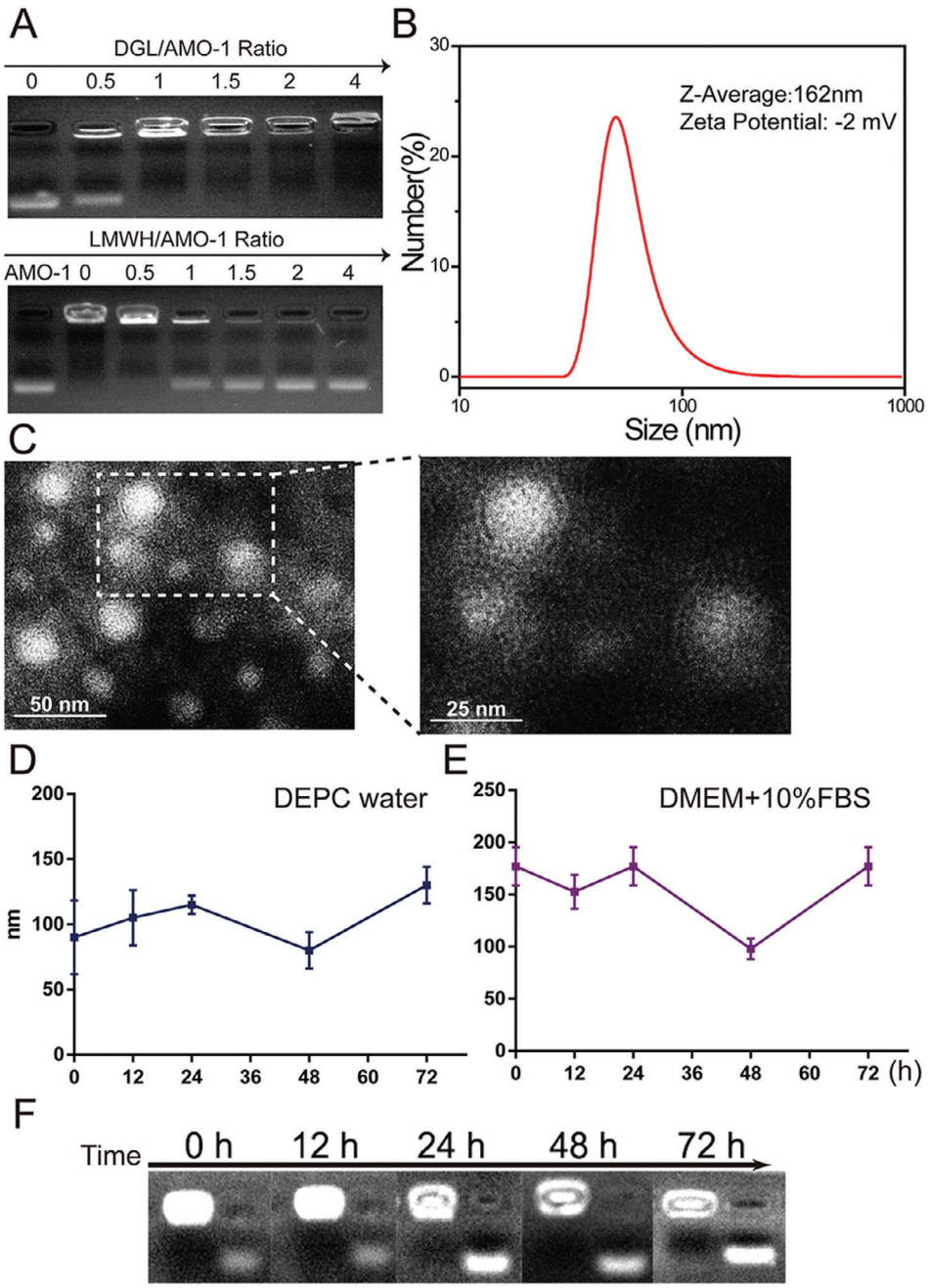

Figure 2. Characterization of HDA NPs. A) Agarose gel electrophoresis evaluation of the appropriate proportion of DGL and LMWH to condense AMO-1. B) Particle size and zeta potentials of HDA. C) Representative AFM images of HDA NPs. D,E) DLS measurement for change in particle size of HDA NPs at the weight ratio of 1:3:2 during 72-h storage in DEPC water and DMEM added 10% FBS ($n = 3$). Data are presented as mean ± SD. F) Anti-degradation of AMO-1 by HDA NPs at room temperature for 72 h by electrophoresis. LMWH@DGL/AMO-1: HDA.

Finally, the optimal weight ratio of DGL: AMO-1: LMWH was 3:2:1. dynamic light scattering (DLS) measurements showed that the mean particle size of HDA was about 162 nm. The zeta potential of this nanoparticle was measured at approximately −2 mV, which was close to neutral (**Figure 2**B). The (polymer dispersion index) PDI was 0.084, suggesting a narrow size distribution. It is worth noting that the NPs formed by mixing LMWH and DGL before loading AMO-1 were different from HDA. These NPs had a wide particle size distribution and were not uniform in morphology (Table S1 and Figure S2, Supporting Information). The TEM image showed a spherical morphology with a diameter of 30 nm, which was lower than the hydrodynamic size by DLS due to dehydration (Figure 2C) and exhibited a shell-core structure. The above findings indicate that LMWH is indispensable in the NPs system in this study.

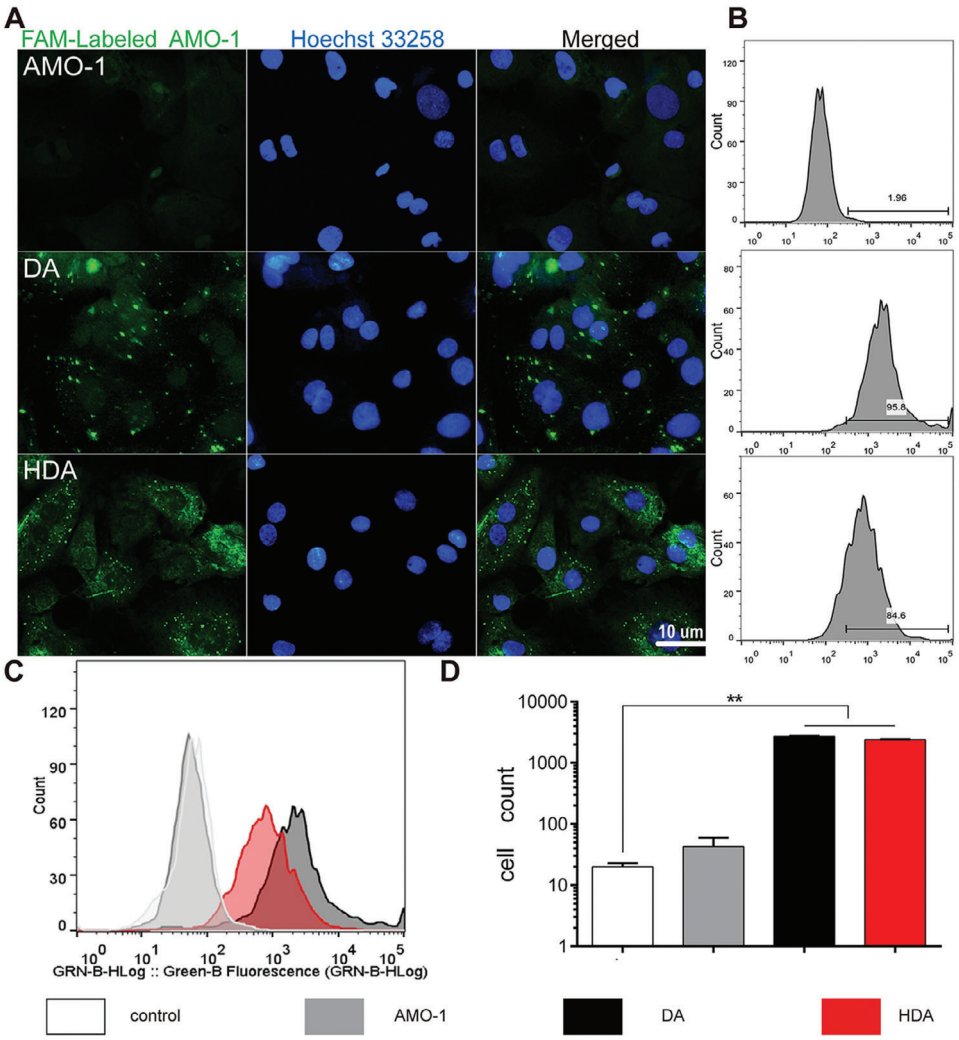

Figure 3. In vitro uptake of AMO-1 or complexed with DGL, LMWH, and DGL in primary cardiomyocytes. A) Fluorescence microscope images of in vitro cellular uptake of AMO-1 mediated by nanocomplexes in primary cardiomyocytes. B,C) Quantitative analysis of flow cytometry was performed after 6-h treatment. Statistical analysis of mean fluorescence intensity of various NPs. D) The counts of primary cardiomyocytes in which various NPs are uptaken. Data are presented as mean ± SD ($n = 3$). *$p < 0.05$, **$p < 0.01$, ***$p < 0.001$. (LMWH@DGL/AMO-1: HDA; DGL/AMO-1: DA.)

HDA stability was investigated by incubation with diethyl pyrocarbonate (DEPC) treated water or DMEM containing 10% FBS at short and long terms. Size change of the complexes was found to be negligible in PBS during 72-h storage (Figure 2D) or DMEM containing 10% FBS during 72-h storage (Figure 2E).

To better assess the intactness of miRNA, the anti-degradation effect of the NPs on the miR-1 inhibitor AMO-1 loaded therein was verified by agarose gel electrophoresis. As shown in Figure 2F, AMO-1 in the HDA placed at room temperature for 72 h could still be replaced by excess LMWH, indicating that AMO-1 could be protected against degradation by the NPs.

2.2. NPs Safety

The cytotoxicity of NPs on rat primary myocardial cells in vitro was assessed by CCK-8 assay. H&E staining was observed to study the safety of HDA after intravenous injection of NPs for 1 month. The detailed results of this part are shown in Figures S4 and S5, Supporting Information.

2.3. Uptake and Intracellular Distribution

The cellular uptake of different AMO-1 formulations with DGL or LMWH and DGL was detected in primary cardiomyocytes after 6-h incubation by flow cytometry and fluorescence microscopy, using carboxyfluorescein (FAM)-labled-AMO-1 products. Fluorescence microscopy showed successful delivery of AMO-1 (green signals) into the cytoplasm to be most effective (**Figure 3**A). At the same time, compared with DA, the introduction of LMWH facilitated uniform dispersion and even distribution of the NPs in cardiomyocytes. The uptake of the complexes was further quantitatively confirmed by flow cytometry in the primary cardiomyocytes after 6-h incubation. It is reported that NPs with a diameter of about 50–200 nm are generally taken up by cells faster

than oversized or small-sized NPs due to the size of clathrin-coated pits and cryptic cell membrane invagination (50–200 nm in diameter).[16] Compared with the positive charge, the transfection efficiency only slightly reduced probably due to the proper size of the HDA.[17]

More interestingly, HDA showed the strongest protective effect on the pulsation of the primary cardiomyocytes cultured for 12-h under hypoxic conditions of 1% oxygen (Video S1, Supporting Information). Flow cytometry detection of FAM-labeled AMO-1 showed that the mean fluorescence intensity of FAM was 76.5 ± 4.3 for PBS, 104.3 ± 33.5 for free AMO-1, 5448 ± 569.9 for DA complex, and 1344.5 ± 57.3 for HDA complex (Figure 3B). Compared with PBS and free AMO-1 groups, the fluorescence intensity of the DA group was increased by 70.2 and 51.2 times respectively. The data also showed that the uptake of the DA complex was four times that of the HDA complex. Further analysis showed that the percentage of FAM-positive cells in the DA and HDA groups was 95.8% and 84.6% respectively (Figure 3D), showing that the uptake efficiency of the HDA complex was slightly reduced. However, the high transfection efficiency was accompanied with a significant damage to the cell viability of the DA complex (Figure S4, Supporting Information).

2.4. Anticoagulative Effect

HDA NPs and DA NPs were injected into the rats through the tail vein, and the size of thrombus formation in vitro was first compared with the saline group and the LMWH group. As shown in **Figure 4**A, the thrombus formed in the DA group was the largest of the four groups, which is consistent with the finding of the previous study that some cationic polymers may activate the blood coagulation reaction in plasma.[18] The thrombus formed in the LMWH group was the smallest, and there is not much difference in the HDA group, indicating that the clinically used anticoagulative LMWH can still exert a certain anticoagulative effect after forming HDA. Next, the commonly used anticoagulative indicators activated partial thromboplastin time (APTT) and prothrombin time (PT) were used to evaluate the anticoagulative effect in vivo. APTT in the HDA group was slightly lower than that in the LMWH group, but it was still 1.72 times that of the saline control group (Figure 4B). No significant difference in PT was observed between the four groups (Figure 4C). Because the rat coronary arteries are too small to be observed clearly, we used the carotid thrombosis model instead to observe the effect of NPs on arterial wall thrombosis. As mentioned above, the entire lumen was filled with thrombi in the DA and saline groups, while HDA showed the antithrombotic ability consistent with LMWH (Figure 4D). The anticoagulative effect of LMWH was evident due to its inhibitory effect on factor Xa. As shown in Figure 4E, LMWH-modified NPs could also exert FXa inhibition regardless of AMO-1.[19]

2.5. In Vivo Evaluation of the Accumulated Effect of AMO-1 in Rat Heart Tissues

In vivo accumulation of Cy3-AMO-1 in the rat heart tissues and sections was observed and imaged (**Figure 5**A). Almost no fluorescence was observed in the exposed miR-Cy3 group and the fluorescence signal was mainly concentrated on the occluded coronary level, which was similar to the finding in the DA group. The heart tissues and sections of the rats treated with HDA-Cy3 showed stronger fluorescence intensity, with the fluorescence penetrating into the infarct area, indicating that DGL could protect AMO-1 against degradation, but only adding the LMWH coating could help the entry of NPs into the lesion. The miR-1 in the infarcted margin of the HDA group was most significantly downregulated, further confirming that AMO-1 in HDA played a role (Figure 5B). Correspondingly, the myocardial infarct size was also the smallest in the HDA group (Figure 5C).

2.6. Anti-Apoptotic Effect in Rats 3 Days after MI

To explore whether HDA could protect the infarcted myocardium, anti-inflammatory and anti-apoptotic effects were evaluated. Knowing that the initial damage characteristic of MI is inflammatory response associated with locally produced cytokines, IL-1β is an early pivotal cytokine,[20] and IL-1β inhibition can prevent myocardial injury,[21] we measured plasma IL-1β at 2 h, 3 and 21 days after MI. It was found that the level of IL-1β in HDA-treated rats was significantly decreased at 2 h after MI, and the NPs without AMO-1 also showed certain inhibitory action on IL-1β, indicating that NPs modified by LMWH had an anti-inflammatory effect. LMWH can block NF-κB pathway to prevent the release of inflammatory mediator.[22] Perhaps this is one of the reason why HDA or HD NPs have the anti-inflammatory effect. However, there was no significant difference in the inhibitory effect of IL-1β in each group at 3 days or 21 days after MI (**Figure 6**A).

Cardiomyocyte apoptosis is one of the major damages in MI.[23] In this study, we used TUNEL staining to identify apoptotic cardiomyocytes and found that there were fewer apoptotic cells in rats treated with NPs with LMWH outer shells as compared with the untreated MI rats, and the apoptotic cells were further reduced after loading AMO-1. To study the anti-apoptosis mechanism, apoptosis-related proteins Bcl-2, Bax, and caspase-3 were analyzed.[24] As shown in Figure 6B,C, the expression of pro-apoptotic proteins Bax and caspase-3 was inhibited and the expression of anti-apoptotic proteins Bcl-2 was upregulated in MI rats treated with HDA. The HD group exhibited a limited effect, indicating that AMO-1 in the NPs is the protagonist of the anti-apoptosis effect.

2.7. Effect on Cardiac Function and Remodeling after MI

Early rescue of the myocardial tissue is important in the treatment of MI, but the preservation of cardiac function after MI and reduction of ventricular remodeling also have a profound impact on long-term prognosis.[25] Cardiac functions were examined 21 days after MI by echocardiography (**Figure 7**A), showing that the LMWH-modified NPs performed well in restoring left ventricle ejection fraction (LVEF) and left ventricle fractional shortening (LVFS). M-mode ultrasound showed that the myocardial wall of the infarction site was less thickened and the contractile performance was improved in the HDA group as compared with

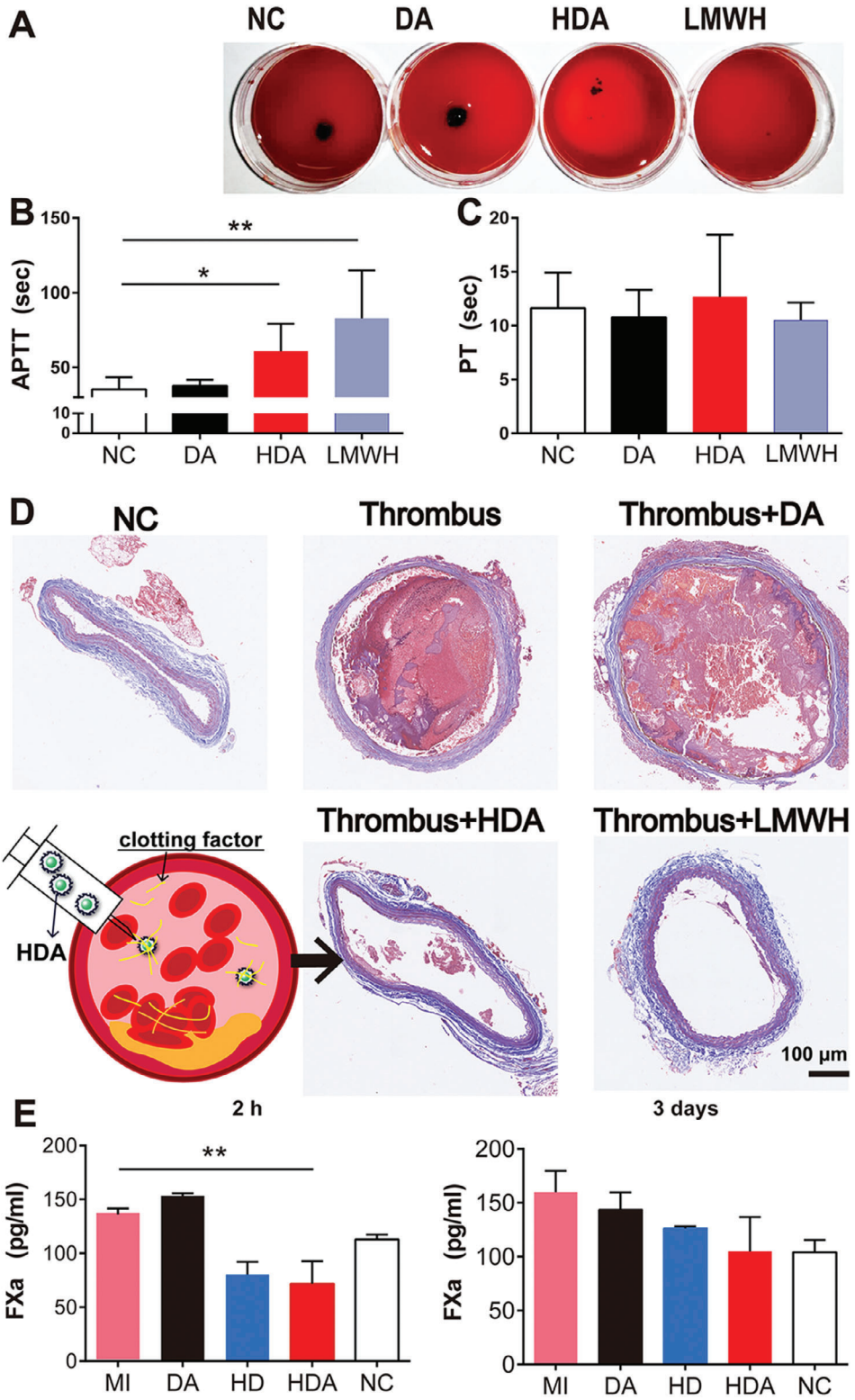

Figure 4. Evaluation of the anti-coagulative effect of HDA in vivo on MI rats. A) Thrombi of different sizes formed 15 min after blood collection from differently treated rats. B) APTT of HDA NPs in vivo. C) PT of HDA NPs in vivo. D) Carotid masson staining. E) FXa expression after MI. LMWH@DGL/AMO-1: HDA; LMWH@DGL: HD; DGL/AMO-1: DA; MI: myocardial infarction rats administrated with saline; NC: normal rats administrated with saline as a control. Data are presented as mean ± SD ($n = 6$). *$p < 0.05$, **$p < 0.01$, ***$p < 0.001$.

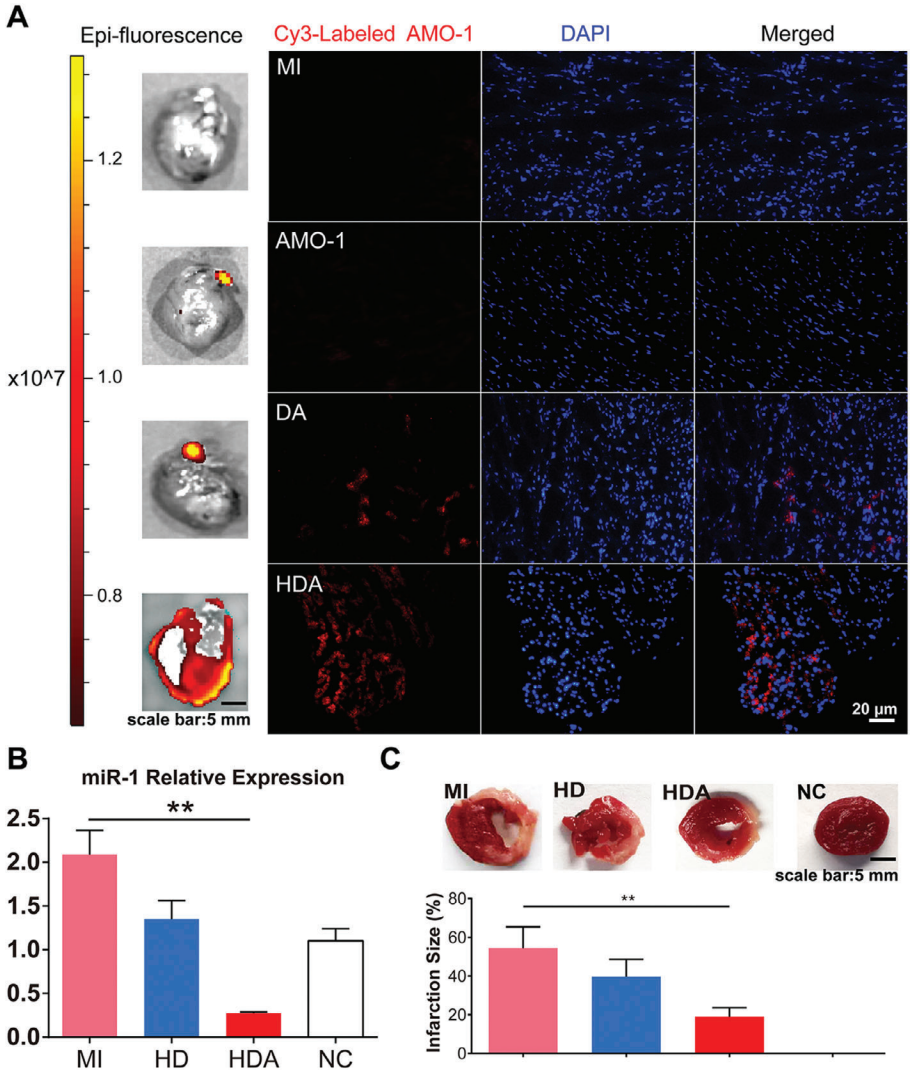

Figure 5. In vivo evaluation of the accumulated effect of AMO-1 in the rat heart tissue. A) Fluorescence images of accumulated AMO-1-Cy3 in the rat heart tissue. B) miR-1 quantification through real-time RT-PCR. C) Cardiac infarct areas determined by TTC-stained heart sections. LMWH@DGL/AMO-1: HDA; LMWH@DGL: HD; DGL/AMO-1: DA; MI: myocardial infarction rats administrated with saline; NC: normal rats administrated with saline as a control. Data are presented as mean ± SD ($n = 6$). *$p < 0.05$, **$p < 0.01$, ***$p < 0.001$.

the non-loaded AMO-1 NPs group. Next, the sirius red stained heart sections were used to observe the degree of cardiac fibrosis. As shown in Figure 7B, the LMWH-modified NPs attenuated cardiac fibrosis, and the HDA group performed the best in this respect.

2.8. Histological Assessment after MI

Angiogenesis plays a pivotal role in preserving cardiac functions and improving the prognosis of ischemic hearts.[26] The amount of neovascularization in the infarcted myocardium of the HDA group was significantly increased, and the formation of new blood vessels was also promoted in the HD group. Interestingly, although there was a certain amount of angiogenesis in the MI group, the diameter of the vessel was large and the shape was irregular (**Figure 8**B). It is speculated that the LMWH-modified nanoparticles may not only promote angiogenesis but also regulate vascular morphology, which needs further study.

Cardiac fibrosis is often accompanied with excessive collagen production and an increase in smooth muscle actin (α-SMA).[27] Figure 8C shows that LMWH-modified NPs (HD) could inhibit the protein expression of Collagen-I and α-SMA even without loading AMO-1. It is certain that the NPs loaded with AMO-1 act more strongly. Fibrosis may be associated with both chronic inflammation and microthrombosis.[28] LMWH has a role in both aspects, which may give HD NPs an anti-fibrosis ability. MiR-1 alleviated the myocardial fibrosis by enhancing mitochondrial NADH dehydrogenase 1 and cytochrome c oxidase I, which may be the reason why HDA shows stronger inhibition of myocardial fibrosis than HD.[29] In simple terms, HDA can improve ventricular remodeling by promoting neovascularization and inhibiting fibrotic protein expression.

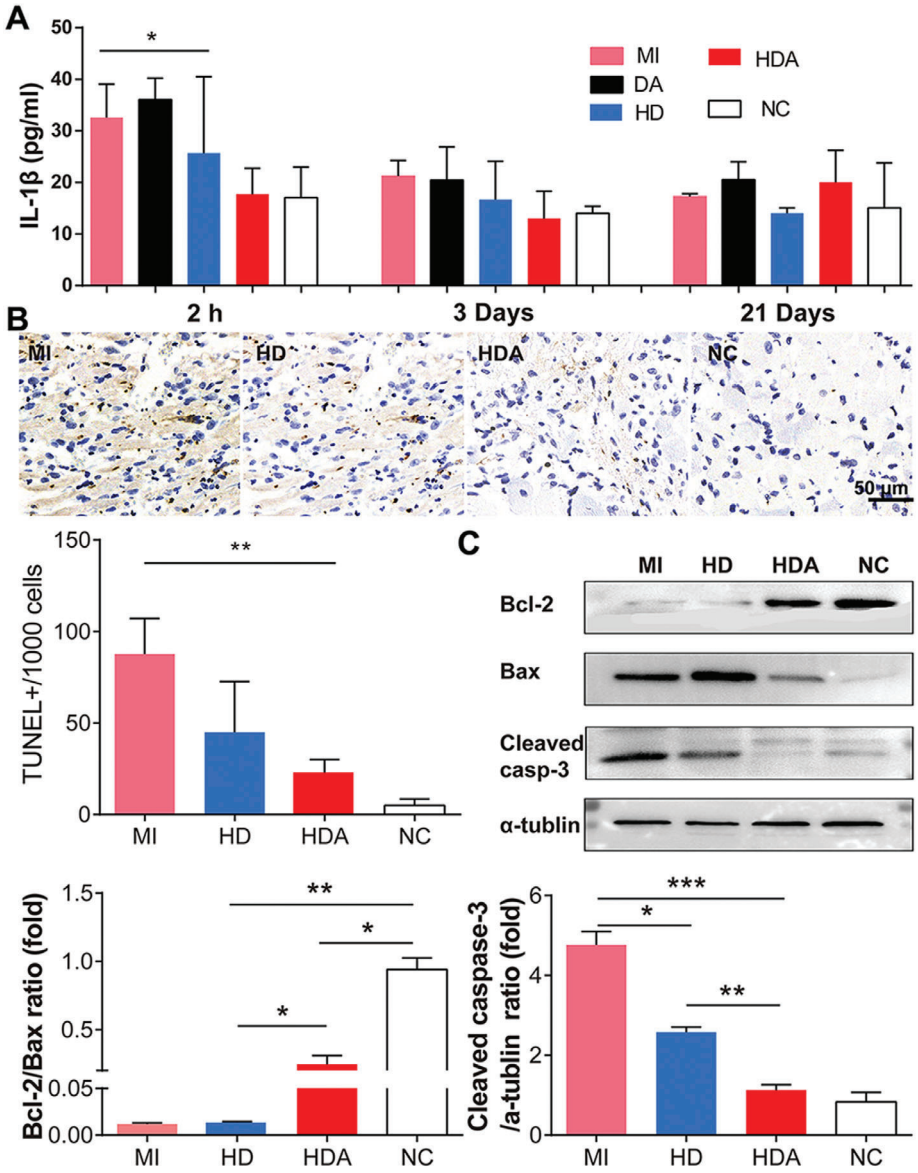

Figure 6. Anti-apoptotic effect in MI rats. A) Changes in the level of inflammatory factor IL-1β at different times after MI. B) TUNEL staining and statistical analysis of the extent of apoptosis in the myocardium. C) Western blot quantification of the level of Bcl-2 and Bax in different groups, expressed as a relative ratio of Bcl-2/Bax, and the western blot quantification of the level of cleaved Caspase-3 in different groups. The intensity of each band was normalized to the intensity of the band for α-tublin, which was used as an internal standard, and expressed as a ratio of relative band intensity. LMWH@DGL/AMO-1: HDA; LMWH@DGL: HD; DGL/AMO-1: DA; MI: myocardial infarction rats administrated with saline; NC: normal rats administrated with saline as a control. Data are presented as mean ± SD ($n = 6$). *$p < 0.05$, **$p < 0.01$, ***$p < 0.001$.

3. Conclusions

We have successfully developed a novel type of low-cytotoxic delivery vehicle, which is able to overcome the problem of microvascular obstruction in AMO-1 delivery. The NPs described herein had a core–shell nanocomplex using DGL-loaded AMO-1 as the core and LMWH as the shell, which exhibited excellent stability and dispersion. Consistent with our expectation, HDA exerted its anticoagulative effect by reducing microthrombus formation. It was subsequently verified to promote AMO-1 delivery to the infarcted area and increased the accumulation of AMO-1 in the infarcted site. To overcome microvascular obstruction, the exploration of AMO-1 loaded NPs with anticoagulative capacity may provide a new miRNA delivery strategy for better treatment of MI.

4. Experimental Section

Materials: AMO-1 labeled with fluorescent dye FAM or Cy3 were synthesized and characterized by Shanghai GenePharma Co., Ltd. The third generation DGL was purchased from Colcom, France. LMWH was

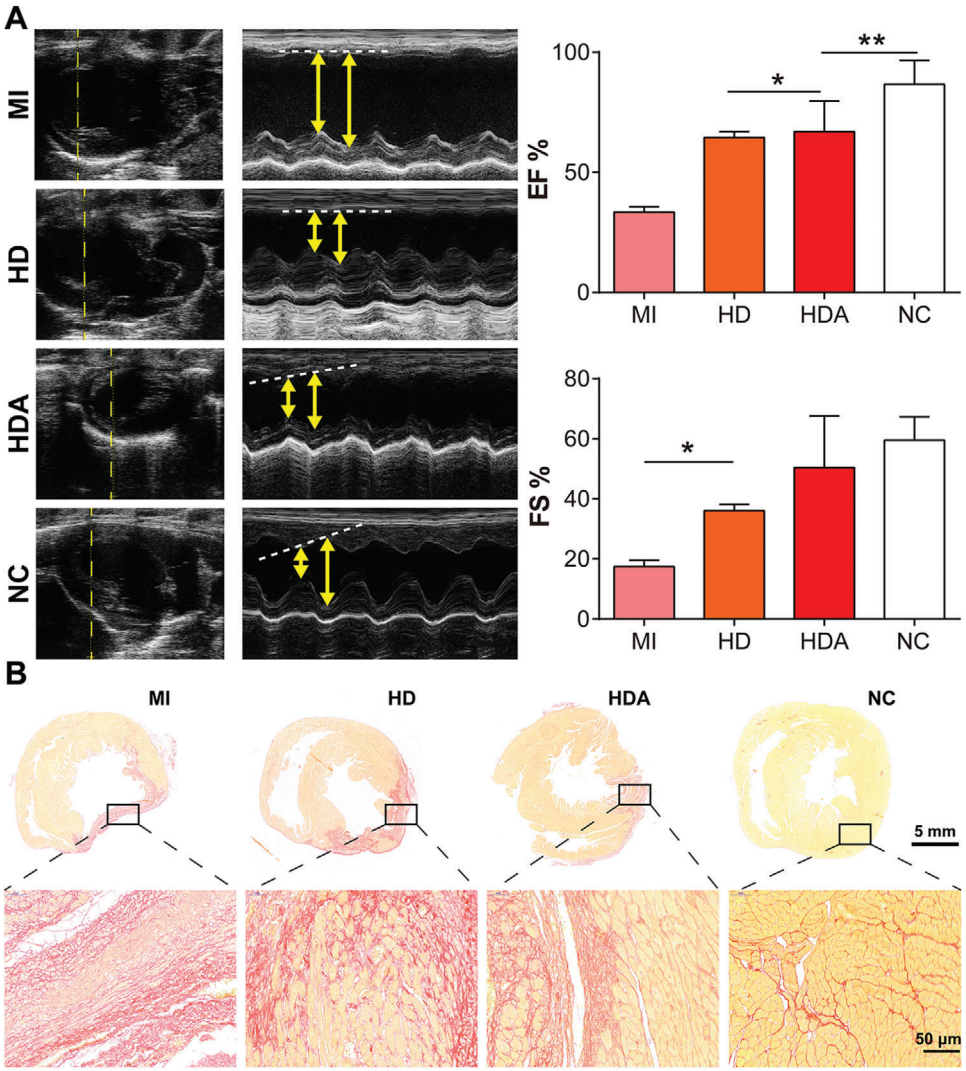

Figure 7. Effect on cardiac function and remodeling after MI. A) M-mode echocardiograms and related LVEF and LVFS. B) Representative Sirius–Scarlet stained histological sections. Normal myocardial tissue (yellow); fibrotic tissue (red). LMWH@DGL/AMO-1: HDA; LMWH@DGL: HD; DGL/AMO-1: DA; MI: myocardial infarction rats administrated with saline; NC: normal rats administrated with saline as a control. Data are presented as mean ± SD ($n = 6$). *$p < 0.05$, **$p < 0.01$, ***$p < 0.001$.

obtained from Dalian Meilun Biological Technology Co., Ltd. Diethyl pyrocarbonate (DEPC)-treated water was purchased from Beijing Solarbio Science & Technology Co., Ltd. GelRed nucleic acid gel stain was purchased from Biotium Inc. (Hayward, CA). Iron chloride ($FeCl_3$, AR, 98%) was supplied by Aladdin Industrial Inc. 2,3,5-triphenyltetrazoliam chloride (TTC) was purchased from Sigma–Aldrich Chemical Co. All antibodies in this experiment used for protein determination were purchased from Cell Signaling Technology, Inc.

Synthesis and Characterizations of HDA: DGL@AMO-1 (DA) was synthesized via electrostatic interaction between DGL and AMO-1 under mild conditions. DEPC-treated water was used for miRNA complexes. Nucleic acid condensability was first tested by agarose gel electrophoresis. Agarose gel electrophoretic analysis was performed to assess whether AMO-1 was complexed fully by DGL. AMO-1 diluted solution was slowly added dropwise to the DGL solution. The DA complexes were prepared at a weight ratio of 0.5:1, 1:1, 2:1, and 4:1. The gel was made of 1.5% (w/v) agarose in TAE buffer containing GelRed. The complexes were mixed with 6 × DNA loading buffer on the gel and electrophoresed for 10 min at 100 V in TAE. Then the location of AMO-1 was visualized under UV excitation using a GelDoc system (Imago). The optimized feed ratio of AMO-1 to DGL was set as 1.5:1 and the reaction was conducted at 37 °C. HDA was prepared by setting LMWH/AMO-1 weight ratios of 0.5:1, 1:1, 1.5: 1, 2:1, and 4: 1. In order to make LMWH a shell of DGL/AMO-1, LMWH was added dropwise to DGL/AMO-1. HDA was successfully synthesized by stirring the mixture. Similarly, agarose gel electrophoresis was performed to find the optimal ratio of LMWH to AMO-1.

The particle size distributions and zeta potentials of HDA and DA were measured by DLS (Zetasizer Nano ZS, ZEN 3690, Malvern). The morphology was observed by transmission electron microscopy (TEM, Tecnai-12 Bio-Twin, FEI, Netherlands).

Biological Stability of HDA: To evaluate the biological stability of HDA, changes in HDA size in DEPC water and DMEM were monitored in the presence of 10% FBS at 4 °C for 72 h. To further verify the anti-degradation effect of the NPs on AMO-1, excess LMWH was added to the sample and observed within 72 h to see whether there was AMO-1 in the agarose gel.

Extraction and Culture of Primary Cardiomyocytes: The ventricles were excised from 2-day-old SD rats, washed, cut into pieces smaller than $1mm^3$, and incubated overnight at 4 °C in D-Hanks' balanced salt solution

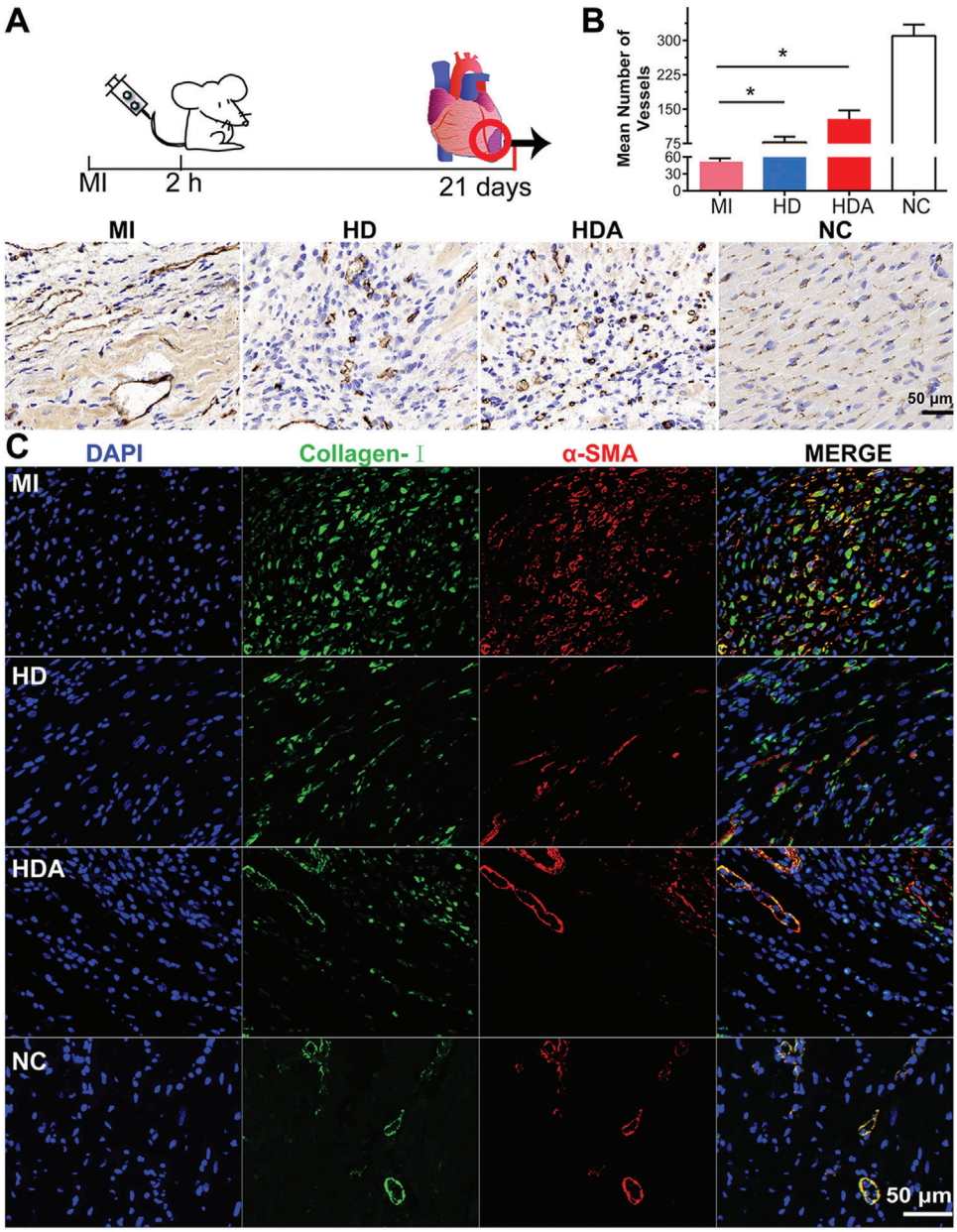

Figure 8. Histological assessment of angiogenesis and fibrotic protein expression 21 days after MI in rats treated with HDA NPs. A) Study design. B) The harvested hearts were sectioned and stained with antibodies against CD31 for endothelial cells. C) Representative microscopic images of fibrotic protein collagen-I and α-SMA expression in the ischemic myocardium 21 days after MI. Collagen-I (green, FITC); nucleus (blue, DAPI); α-SMA (red, Cy-3). LMWH@DGL/AMO-1: HDA; LMWH@DGL: HD; DGL/AMO-1: DA; MI: myocardial infarction rats administrated with saline; NC: normal rats administrated with saline as a control. Data are presented as mean ± SD ($n = 6$). *$p < 0.05$, **$p < 0.01$, ***$p < 0.001$.

containing 0.5% trypsin. The small pieces were then collected and further digested in type-II collagenase (100 units mL^{-1}; Worthington, USA) for 40 min at 37 °C. The digestion was terminated with DMEM (Gibco-Life) supplemented with 10% FBS, and the small pieces were re-suspended by pipetting. The resulting cell suspensions were filtered through a cellular sifter (200-mesh), and incubated in DMEM with 10% FBS for 70 min. Cells in suspension were removed and the remaining cells attached to the bottom were collected, re-plated at a density of 3–5 × 10^5 cells mL^{-1}, and cultured in DMEM with 10% FBS, 100 units mL^{-1} penicillin, 100 μg mL^{-1} streptomycin, and 0.1 mM bromodeoxyuridine. As estimated by staining of α-actinin, the purity of cardiomyocytes was >90%. All animal care and experimental procedures were complied with the regulations of the ethics committee of Shanghai Jiaotong University School of Medicine (Shanghai, China).

Toxicity Evaluation of HDA In Vitro and In Vivo: Primary rat cardiomyocytes cultured in 96-well plates at 8 × 10^3 cells per well were incubated with HDA or DA at predetermined concentrations. After 6, 12, and 24 h, CCK-8 assay was conducted to characterize cytotoxicity of the NPs in vitro.

For in vivo safety consideration, the rat organs were excised and H&E stained to evaluate the possible adverse effects of the NPs. Body weight was recorded every 1 or 2 weeks until sacrifice ($n = 3$).

HDA Uptake and Intracellular Distribution: To investigate the cellular uptake efficacy of the NPs in vitro, primary rat cardiomyocytes were cultured in confocal imaging dishes (3×10^5 per well) and 24-well chamber slides (5×10^4 per well) for 24 h. FAM-labeled different AMO-1 formations were cultured with the cells for 6 h. After removing the medium, cells were dyed with Hochst33258 for 10 min at room temperature, and then gently washed with PBS twice and carefully harvested for fluorescence microscope imaging. The excitation was 525 nm for FAM, and 340 nm for Hochst33258. Flow cytometry (BD Biosciences, USA) was applied to further analyze the fluorescent intensity of the NPs.

Surgical Preparation of the Rat Carotid Thrombosis Model and MI Model: Specific pathogen-free (SPF)-grade male SD rats weighing 200 ± 20 g were fed in a SPF environment in the Laboratory Animal Center of Xinhua Hospital affiliated to Shanghai Jiaotong University School of Medicine. All animal care and experimental procedures complied with the regulations of the ethics committee of Shanghai Jiaotong University School of Medicine (Shanghai, China).

To establish the rat carotid thrombosis model, an incision was made along the midline of the anterior neck after successful induction of anesthesia by continuous inhalation of isoflurane, and the muscles of each layer were bluntly separated to avoid cutting the surrounding blood vessels and exposing the carotid artery. The elbow hemostat was freed from the carotid artery and separated from the jugular vein and the vagus nerve. Thrombosis was initiated by placing a filter paper (1×1 mm^2) soaked in a 15% $FeCl_3$ solution on the exposed carotid surface for 10 min. After removing the filter paper, the carotid artery and its surrounding tissues were washed with a 0.9% saline solution.

To build a MI model, the rat was orally intubated with a 16-gauge tube and ventilated at a respiratory rate of 80 breaths min^{-1} and a tidal volume of 8 mL. After successful induction of anesthesia by continuous inhalation of isoflurane, a left-side thoracotomy was performed to expose the heart. To clearly expose the coronary arteries, the pericardium was first carefully stripped, and then a 5-0 silk suture was passed immediately through the left anterior descending coronary artery near its origin. Ischemia was confirmed by visual inspection of blanching in the myocardium distal to the site of occlusion. Sham-operated animals underwent an identical procedure without ligation.

Evaluation of the Anticoagulative Effect: The animal was injected with saline, DA, HDA, and LMWH as designed at a dose of 0.2 mg AMO-1/0.5 mL saline/rat. Blood was taken from the heart of each group of rats and allowed to stand at room temperature for 20 min, when the thrombus was observed attaching to the wall. To further observe the size of the thrombus, it was gently shaken and then poured into a clean 6-cm cell culture dish. APTT and plasma PT were further tested to demonstrate the anticoagulative effect.

In Vivo Therapeutic Strategy: For different experimental purposes, rats were randomly assigned to a MI group, a MI + DA group, a MI + HD group, and a MI + HDA group, using sham-operated rats as the normal control (NC) group. 2 h after MI surgery, rats in MI +DA group, MI + HD group, and MI + HDA group were injected with DA, HD, and HDA via the tail vein at a dose of 0.2 mg AMO-1/0.5 mL saline/rat. Rats in MI and NC groups were injected with physiological saline. 2 h after the injection, 1 mL blood was taken from the rat heart for plasma extraction. 1 day after the injection, six rats in each group were sacrificed and the heart was taken out for TTC staining. 3 days after administration, six rats in each group were sacrificed to remove the heart for real-time PCR, Western Blot analysis and TUNEL assay. Then, 21 days after the injection, six rats of each group were additionally subjected to cardiac ultrasound function measurement and then sacrificed to perform ventricular remodeling evaluation. To evaluate the ventricular remodeling effect, the heart was sliced for use. Sirius red staining was used to observe the degree of fibrosis. The harvested heart was sliced into sections and stained with antibodies against CD31 against endothelial cells to observe the degree of neovascularization by incubating Cy3-labeled α-SMA antibody, FITC-labeled collagen-I antibody and DAPI with the heart sections for fluorescence imaging and observation of fibrotic protein expression.

In Vivo Uptake and Accumulation: A total of 24 rats were randomly assigned to four groups: a MI group, a MI + naked AMO-1 group, a MI+DA group, and a MI+HDA group. 2 h after MI induction, Cy3-labeled AMO-1 was injected via the tail vein at a dose of 0.2 mg per rat in 0.5 mL saline. 12 h after AMO-1 injection, the MI rats were sacrificed and the organs were examined ex vivo by living imaging system to evaluate NPs accumulation in the heart. The heart was then frozen, sliced into sections, incubated with DAPI, and observed for NPs aggregation in the myocardium by fluorescence imaging (red).

Real-Time RT-PCR: Total RNA extracted from the rat heart was converted to cDNA for quantitative PCR using high-capacity cDNA Reverse Transcription Kits (Takara, Japan). The expression level of U6 was quantitated as an internal control according to the TB Green PCR Master Mix (Takara, Japan) manufacturer's instructions. The forward primer of miR-1 for RT-PCR was 5′-GCG GTG GAA TGT AAA GAA GTG TG-3′, and the reverse primer of miR-1 was 5′- ACC GTG TCG TGG AGT CGG CAA TT -3′. The forward primer of U6 was 5′-GGA ACG ATA CAG AGA AGA TTA GC-3′, and the reverse primer of U6 was 5′-TGG AAC GCT TCA CGA ATT TGC G -3′.

Western Blot Assay: Total protein was extracted from the rat LV for immunoblotting analysis. Briefly, the protein sample (50 µg) was separated in SDS-PAGE and blotted to a nitrocellulose membrane. The blots were probed with primary antibodies including Bcl-2 (1:500 dilution, CST), Bax (1:500 dilution, CST), cleaved caspase-3 (1:500 dilution, Abclone) and α-tublin (1:1000 dilution, Beyotime Biotechnology), and then with horseradish peroxidase-conjugated secondary antibody (1:1000 dilution, Beyotime Biotechnology). The Western blot bands were collected by the imaging system (LI-COR Biosciences, Lincoln, NE, USA) and quantitated with image J 5.0 software by measuring intensity (area 6OD) in each group using α-tublin as the internal control.

Detection of Serum Inflammatory Factors: Clotting factor Xa and IL-1β levels in plasma were detected using Rat Quantikine ELISA Kits (Jianglaibio, Shanghai, China), according to the manufacturer's instructions.

Echocardiographic Assessment of Cardiac Function: Transthoracic echocardiography with an ultrasound instrument (Vivid 7 GE Medical) equipped with a 10-MHz phased-array transducer was used to measure the LV function. Interventricular septum diastolic thickness, interventricular septum systolic thickness, LVEF, and FS were calculated from M-mode recording.

Statistical Analysis: Data are presented as the mean ± standard deviation (SD). All results were analyzed with one-way analysis of variance using SPSS V 21.0 software. 0.05 was considered to show a statistically significant difference. $p < 0.01$ and $p < 0.001$ were considered to indicate a significant or extremely significant difference.

Supporting Information

Supporting Information is available from the Wiley Online Library or from the author.

Acknowledgements

T.H., Y.W., and X.X. contributed equally to this work. This work was supported by National Natural Science Foundation of China (No. 81974292,81671944, and 81470390); Program of Science and Technology Commission of Shanghai Municipality (No. 17411954700); Translational Medicine Cross Research Fund of Shanghai Jiao Tong University (No. ZH2018ZDB01); and Shanghai Sailing Program (19YF1431700).

Conflict of Interest

The authors declare no conflict of interest.

Keywords

low molecular weight heparin, microvascular obstructions, miRNA, myocardial infarctions, nanodelivery

Received: December 12, 2019
Revised: March 9, 2020
Published online:

[1] a) S. N. Hayes, E. S. H. Kim, J. Saw, D. Adlam, C. Arslanian-Engoren, K. E. Economy, S. K. Ganesh, R. Gulati, M. E. Lindsay, J. H. Mieres, S. Naderi, S. Shah, D. E. Thaler, M. S. Tweet, M. J. Wood, *Circulation* **2018**, *137*, e523; b) H. Thomas, J. Diamond, A. Vieco, S. Chaudhuri, E. Shinnar, S. Cromer, P. Perel, G. A. Mensah, J. Narula, C. O. Johnson, G. A. Roth, A. E. Moran, *Global Heart* **2018**, *13*, 143.

[2] a) Y. Zhang, Z. Wang, R. A. Gemeinhart, J. Control, *J. Controlled Release* **2013**, *172*, 962; b) R. A. Boon, S. Dimmeler, *Nat. Rev. Cardiol.* **2015**, *12*, 135; c) T. F. Luscher, *Eur. Heart J.* **2017**, *38*, 2517.

[3] T. Bejerano, S. Etzion, S. Elyagon, Y. Etzion, S. Cohen, *Nano Lett.* **2018**, *18*, 5885.

[4] a) Y. Tang, J. Zheng, Y. Sun, Z. Wu, Z. Liu, G. Huang, *Int. Heart J.* **2009**, *50*, 377; b) J. N. Tsoporis, A. Fazio, I. K. Rizos, S. Izhar, G. Proteau, V. Salpeas, A. Rigopoulos, E. Sakadakis, I. K. Toumpoulis, T. G. Parker, *J. Mol. Cell. Cardiol.* **2018**, *121*, 25; c) Y. Wu, T. Wang, X. Sun, *Int. J. Cardiol.* **2018**, *257*, 275.

[5] X. Xue, X. Shi, H. Dong, S. You, H. Cao, K. Wang, Y. Wen, D. Shi, B. He, Y. Li, *Nanomedicine* **2018**, *14*, 619.

[6] a) G. L. D. Maria, F. Cuculi, N. Patel, S. Dawkins, G. Fahrni, G. Kassimis, R. P. Choudhury, J. C. Forfar, B. D. Prendergast, K. M. Channon, R. K. Kharbanda, A. P. Banning, *Eur. Heart J.* **2015**, *36*, 3165; b) P. Libby, G. Pasterkamp, F. Crea, I. K. Jang, *Circ. Res.* **2019**, *124*, 150.

[7] M. J. Davies, A. Thomas, *N. Engl. J. Med.* **1984**, *310*, 1137.

[8] P. Libby, *N. Engl. J. Med.* **2013**, *368*, 2004.

[9] D. P. J. Kavanagh, A. B. Lokman, G. Neag, A. Colley, N. Kalia, *Cardiovasc. Res.* **2019**, *115*, 1918.

[10] Y. H. Bae, K. Park, *J. Controlled Release* **2011**, *153*, 198.

[11] a) J. Chandrasekhar, R. Mehran, *Prog. Cardiovasc. Dis.* **2015**, *58*, 247; b) B. Ibanez, S. James, S. Agewall, M. J. Antunes, C. Bucciarelli-Ducci, H. Bueno, A. L. P. Caforio, F. Crea, J. A. Goudevenos, S. Halvorsen, G. Hindricks, A. Kastrati, M. J. Lenzen, E. Prescott, M. Roffi, M. Valgimigli, C. Varenhorst, P. Vranckx, P. Widimsky, *Eur. Heart J.* **2018**, *39*, 119.

[12] a) S. Ali-Hassan-Sayegh, S. J. Mirhosseini, A. Shahidzadeh, P. Mahdavi, M. Tahernejad, F. Haddad, M. R. Lotfaliani, A. Sabashnikov, A.-F. Popov, *Indian Heart J.* **2016**, *68*, 213; b) F. Franchi, F. Rollini, D. J. Angiolillo, *Nat. Rev. Cardiol.* **2017**, *14*, 361.

[13] D. A. Garcia, T. P. Baglin, J. I. Weitz, M. M. Samama, *Chest* **2012**, *141*, e24S.

[14] C. Passirani, G. Barratt, J. P. Devissaguet, D. Labarre, *Life Sci.* **1998**, *62*, 775.

[15] X. Yang, H. Du, J. Liu, G. Zhai, *Biomacromolecules* **2015**, *16*, 423.

[16] a) S. Prabha, W. -Z. Zhou, J. Panyam, V. Labhasetwar, *Int. J. Pharm.* **2002**, *244*, 105; b) G. J. Doherty, H. T. McMahon, *Annu. Rev. Biochem.* **2009**, *78*, 857; c) A. Kumari, S. K. Yadav, *Expert Opin. Drug Delivery* **2011**, *8*, 141.

[17] B. Wang, L. Zhang, S. C. Bae, S. Granick, *Proc. Natl. Acad. Sci. USA* **2008**, *105*, 18171.

[18] C. Sperling, M. F. Maitz, S. Grasso, C. Werner, S. M. Kanse, *ACS Appl. Mater. Interfaces* **2017**, *9*, 40107.

[19] M. Alhenc-Gelas, C. J. Guernic, J. F. Vitoux, A. Kher, M. Aiach, J. N. Fiessinger, *Thromb. Haemostasis* **1994**, *71*, 698.

[20] a) M. Kawaguchi, M. Takahashi, T. Hata, Y. Kashima, F. Usui, H. Morimoto, A. Izawa, Y. Takahashi, J. Masumoto, J. Koyama, M. Hongo, T. Noda, J. Nakayama, J. Sagara, S. Taniguchi, U. Ikeda, *Circulation* **2011**, *123*, 594; b) J. Yin, Y. Wang, H. Hu, X. Li, M. Xue, W. Cheng, Y. Wang, X. Li, N. Yang, Y. Shi, S. Yan, *J. Cell. Mol. Med.* **2017**, *21*, 2695.

[21] B. J. Pomerantz, L. L. Reznikov, A. H. Harken, C. A. Dinarello, *Proc. Natl. Acad. Sci. USA* **2001**, *98*, 2871.

[22] F. Ning, X. Wang, L. Shang, T. Wang, C. Lv, Z. Qi, D. Wu, *Gene* **2015**, *557*, 88.

[23] D. P. D. Re, D. Amgalan, A. Linkermann, Q. Liu, R. N. Kitsis, *Physiol. Rev.* **2019**, *99*, 1765.

[24] J. Li, H. P. Hu, Y. Li, W. Shao, J. Z. Zhang, L. M. Wang, *Eur. Rev. Med. Pharmacol. Sci.* **2018**, *22*, 8951.

[25] E. B. Schelbert, Y. Fridman, T. C. Wong, H. Abu Daya, K. M. Piehler, A. Kadakkal, C. A. Miller, M. Ugander, M. Maanja, P. Kellman, D. J. Shah, K. Z. Abebe, M. A. Simon, G. Quarta, M. Senni, J. Butler, J. Diez, M. M. Redfield, M. Gheorghiade, *JAMA Cardiol.* **2017**, *2*, 995.

[26] L. Luo, J. Tang, K. Nishi, C. Yan, P. U. Dinh, J. Cores, T. Kudo, J. Zhang, T. S. Li, K. Cheng, *Circ. Res.* **2017**, *120*, 1768.

[27] a) V. V. Petrov, R. H. Fagard, P. J. Lijnen, *Hypertension* **2002**, *39*, 258; b) C. J. Li, L. Lv, H. Li, D. M. Yu, *Cardiovasc. Diabetol.* **2012**, *11*, 73.

[28] a) C. Li, Z. Yang, X. Shi, D. Liu, *World J. Gastroenterol.* **2017**, *23*, 6412; b) J. M. Vieira, S. Norman, C. V. D. Campo, T. J. Cahill, D. N. Barnette, M. Gunadasa-Rohling, L. A. Johnson, D. R. Greaves, C. A. Carr, D. G. Jackson, P. R. Riley, *J. Clin. Invest.* **2018**, *128*, 3402.

[29] R. He, C. Ding, P. Yin, L. He, Q. Xu, Z. Wu, Y. Shi, L. Su, *Exp. Cell Res.* **2019**, *378*, 87.